Materials & Design 225 (2023) 111420

Contents lists available at ScienceDirect

Materials & Design

journal homepage: www.elsevier.com/locate/matdes

# Development of a high-performance cutting device based on hybrid actuation for ultra-precision machining

Zhuoxuan Zhuang [a], Hanheng Du [a], Wai Sze Yip [a], Tengfei Yin [a], Zejia Zhao [c], Zhiwei Zhu [b], Suet To [a,*]

[a] State Key Laboratory of Ultra-precision Machining Technology, Department of Industrial and Systems Engineering, The Hong Kong Polytechnic University, Kowloon, Hong Kong Special Administrative Region
[b] School of Mechanical Engineering, Nanjing University of Science and Technology, Nanjing 210094, JS, China
[c] Institute of Semiconductor Manufacturing Research, College of Mechatronics and Control Engineering, Shenzhen University, Shenzhen 518060, Guangdong, China

## HIGHLIGHTS

- Hybrid actuation for microstructure generation.
- High working frequency (3300 Hz) of flexure-hinge compliant mechanism.
- Optimizing customized designed voice coil motor by magnetic simulation.
- Validating the performance of the designed hybrid cutting device by machining microstructure.

## GRAPHICAL ABSTRACT

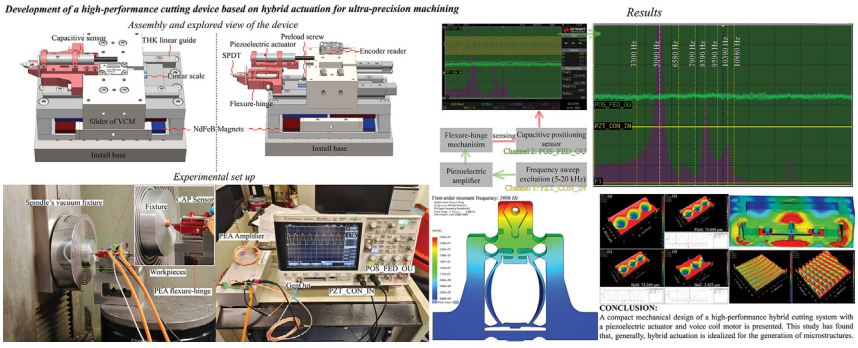


## ARTICLE INFO

*Article history:*
Received 14 October 2022
Revised 18 November 2022
Accepted 21 November 2022
Available online 23 November 2022

*Keywords:*
Linear voice coil motor
Piezoelectric actuator
Flexure-hinge
Microstructure
Ultra-precision cutting

## ABSTRACT

In ultra-precision cutting, the inherent working frequency and positioning accuracy of actuators are decisive. It is challenging to generate multi-scale cutting motions with high accuracy on hierarchical scale simultaneously. In this study, a novel micro and nano-cutting device with complex-axis is developed, consisting of a customized designed linear voice coil motor and a piezoelectric actuated flexure-hinge mechanism to generate micro and nano-cutting motions, respectively, for overcoming the challenge. The structure of the cutting device is designed with a small form factor in dimension in comparison to other auxiliary cutting devices for ultra-precision machine tools. The magnetic field simulation is also used to optimize the output force of the voice coil motor with the simulation results validated by experiments using a force sensor. The operation mechanism of the flexure-hinge is investigated by finite element analysis. The device can perform ± 0.5 mm stroke at 10 Hz and ± 8 μm at 3300 Hz for generation of microstructures with experimental validation. The significance and originality of this study lie in the successful development of a novel hybrid actuation cutting system that can generate multi-scale cutting motions with high accuracy and flexibility on a hierarchical scale for the generation of microstructured surfaces in ultraprecision machining.


## 1. Introduction

Flexure-hinge-based compliant mechanism or voice coil motor (VCM) actuated fast tool servo (FTS) is an effective auxiliary machining technique for micro/nanostructure generation in

* Corresponding author.
*E-mail address:* sandy.to@polyu.edu.hk (S. To).

https://doi.org/10.1016/j.matdes.2022.111420
0264-1275/

ultra-precision diamond turning [1,2]. Different kinds of FTS devices were developed in response to specific requirements. Trumper et al. [3] summarized different FTS systems categorized by actuators, including normal-stress electromagnetically-driven, Lorentz force, magnetostrictive, hydraulic, and piezoelectric actuators. Bandwidth, positioning accuracy, and stroke of the cutting system are inherent to a limited spectrum as a result of actuators belonging to particular categories. The conventional actuator for the FTS system is typically a VCM or piezoelectric actuator, depending on the stroke and working frequency requirements of the system. Several researchers have attempted to overcome these limitations by optimizing the mechanical design[4–6]. Some researchers focused on the development of a novel flexure-hinge amplification mechanism, and it has been demonstrated that a very large amplification ratio of 91 is achieved [7], while the working frequency of this flexure hinge is at about 47.5 Hz. With the limited amplification ratio of the compliant mechanism, the stroke was slightly lengthened at the expense of a significant reduction in working frequency. In comparison to another type of actuator, such as the VCM, the extended stroke of the compliant mechanism is still measured in micron-scale, whereas the travel range of the VCM is measured in millimetre-scale. Although there are scientific articles discussing the results of amplification ratios in compliant mechanisms, the majority of the results have limited macroscale strokes[8,9]. The most significant disadvantage of this type of cutting system for the generation of hierarchical micro/nanostructure is that the improved performance in strokes typically results in a decrease in the working frequency of the flexure-hinge-based compliant mechanism.

The balance between working frequency and travel range is a classic problem in ultra-precision cutting devices used for generating microstructures. In recent years, there has been a surge of interest in the development of high-performance cutting devices. A novel FTS based on VCM with embedded counterbalance technology has significantly improved the system performance in tracking error aspect under the ± 1 mm (±0.5 mm) stroke at 30 Hz (40 Hz) with 0.35 % (0.68 %) [10]. Gong et al. [11] developed a novel long-stroke cutting device actuated by the VCM and an air-bearing guiding system, with a stroke ranging from ± 0.1 to ± 1.5 mm and a bandwidth of 100 Hz. Zhu et al. [12] developed a flexure-hinge mechanism-based nanometric ultra-FTS for nanostructure cutting that achieved a quasi-static stroke of 6 μm and a travel range of 1.2 μm with a bandwidth of 10 kHz. The stroke of the VCM-driven system is a hundred times that of the flexure-hinge-based cutting device, while the working frequency of the VCM-actuated cutting device is only one percent of the flexure-hinge-based compliant mechanism. To overcome the drawbacks of the piezoelectric-actuated cutting system, Tian et al. [13] developed a novel long-stroke cutting system based on the VCM for the diamond turning process. They also developed a VCM-based cutting system with a long stroke of 30 mm and a high acceleration of 920 $m/s^2$ to extend the bandwidth of the system [14].

Many researchers have investigated the control technique for the VCM and piezoelectric actuated cutting device. Tao et al. [15] presented a VCM-based cutting system with a self-sensing technique for cutting force in which the resolution can be achieved at five mN. Force sensing technology is also employed in the piezoelectric actuated cutting device, Zhou et al. [16] applied a mechanical observer within the flexure chain of their force sensing cutting device, the bandwidth of force sensing is 600 Hz, and the resolution is approximately 0.24 mN. Moreover, an online constructive fuzzy sliding mode has been developed. This control algorithm enables the VCM sliding-mode system to achieve precise position tracking [17]. Some researchers prototyped an embedded displacement sensor within the VCM based on the displacement proportional to the ampere force of its specified guide system [18]. These designs could reduce system costs and enhance the control performance for fabricating the microlens array. Regarding the enhancement of the control strategy, Wu et al. [19] developed an active disturbance rejection controller that improves the tracking accuracy of the VCM-based cutting system for noncircular machining. Tian et al. [20] also developed an adaptive feedforward cancellation (AFC) control strategy for the VCM FTS system, achieving perfect tracking and disturbance rejection in periodic control.

In the aspect of the application of the high-performance cutting system in ultra-precision machining, some researchers focused on the degree of freedom (DOF) in flexure-hinge-based FTS, Li et al. [21] developed a 3-DOF piezoelectric FTS for microstructure machining with the stroke of 40 μm and natural frequency of 800 Hz. In the meantime, a novel design of the flexure-hinge-based cutting device for brittle material machining is also investigated. Zhu et al. [22] proposed a tuned diamond turning to precisely match the maximum depth-of-cut during the cutting process, improving the machining efficiency by 16.35 %. Based on the preceding discussion, the high-performance system is frequently consisting of a single actuator, either a VCM or a piezoelectric actuator. This characteristic may determine the stroke size and working frequency. Inspired by these, Zhou et al. [23] have utilized two types of actuators to develop a hybrid actuation cutting system in which the piezoelectric actuated mechanism is designed to compensate for the shortcomings of the high-frequency capacity of the VCM. The defects of the flexure-hinge compliant and VCM actuated cutting system are evident, and integration of these two systems may overcome the weaknesses of the separate system. Actually, hybrid actuation has not been systematically investigated to date. Consequently, the integration of two categories (piezoelectric actuated and VCM driven cutting system) enables good performance in terms of stroke and working frequency, based on findings of separate category actuators from the pioneering researchers.

This paper describes the design and implementation of a hybrid high-performance actuation cutting device for ultra-precision machining microstructures. This study utilized magnetic simulation techniques to develop a linear VCM with a small form factor. In the meantime, finite element modal analysis and experimental validation are also employed for the flexure-hinge compliant mechanism. The performance tests of the VCM actuated slider system are systematically conducted to find out the current step response, sine mode stroke tracking and constant force curve. Finally, the hybrid actuation cutting device was subsequently installed on the Moore 350FG ultra-precision machining tool to validate the cutting performances by generating a specific dimple array. The experimental work presented demonstrates the capabilities of the hybrid actuation in positioning accuracy and working frequency domain. The measurement results of generated microstructure surface were compared to those of the designed surface. Therefore, this study makes a major contribution to research on hybrid actuation cutting systems by demonstrating microstructure generation in ultra-precision machining.

## 2. Conceptual design of the hybrid actuation cutting device

### 2.1. Overview of the hybrid actuation cutting device

According to literature, the actuation cutting systems are generally driven by a single class of actuators, piezoelectrically actuated [21,24,25] or Lorentz force driven [26,27]. Very few studies have investigated hybrid actuation systems for the generation of microstructures in ultra-precision machining. Most studies in the field of the cutting system have only focused on single aspect of improvement. In this study, this device developed is a dual hybrid actuated mechanism that generates both nano/micro motions with

micron/millimetre strokes simultaneously. The central controller modulates first- and second-order tool-patch translated from a hierarchical surface. Collaborating with the primary machine tool computer numerical control system passively through auxiliary linear encoder signal interface, the central controller output two driving commands in differential voltage mode for the VCM amplifier and piezoelectric voltage amplifier, respectively. Two linear stroke systems are sequentially positioned in one direction along the Z-axis. Thus, the device can generate a linear hierarchical motion for the generation of a hierarchical surface during single diamond turning.

Fig. 1 shows two cutting systems installed on a Moore 350FG ultra-precision machine tool base stage. The single point diamond tool (SPDT) is mounted in a flexure-hinge forming fixture. The nano motion is powered by the piezoelectric actuator (PEA, P_887.51, PICMA® Multilayer Piezoelectric Actuator). A nano-resolution capacitive sensor is installed in front of the flexure-hinge mechanical structure to detect deformation. The capacitive sensor sends the controller real-time positioning feedback. The PEA, capacitive sensor, and flexure-hinge compliant mechanical structure produce nano vibrate strokes at high frequencies. This mechanism is capable of producing microscale motion with high precision and excellent dynamic response in the high-frequency domain. The subsystem is therefore an idealized solution for the generation of hierarchical microstructures at the level of the second-order hierarchical microstructures. The sliding system consists of a linear VCM and a linear mechanical guiding system in addition to the flexure-hinge mechanism. The linear optical encoding system is installed on the surface of the VCM stator to provide positioning feedback, as shown in Fig. 1(a). This linear VCM is customized to reduce the weight of the system slider as much as possible to improve the dynamic performance and bandwidth of the first-order actuation system. In addition, the coil of the armature is optimized using magnetic field simulation.

### 2.2. Mechanical design of the voice coil motor

A specially designed VCM is used for generating the first-order stroke with a long-range stroke of 30 mm in total. Considering the form factor, the VCM is installed at the top of the base fixture with a dimension of 114 × 80 × 74 mm, as illustrated in Fig. 2(a). The whole device is tiny for installation on an ultra-precision machine. As depicted in Fig. 2(a), the look-down view size of the device is nearly identical to that of the iPhone4. This small form factor has the advantage of collaboration with most machine tools. The slider of the VCM is guided by a set of linear mechanical guides (model: THK HR918U). The first-order stroke mechanism can achieve nano resolution (50 nm) with X400 interpolation using the Renishaw 20 μm pitch linear encoder system.

High thermal conductivity resin is used to attach an optimized voice coil to the supporting frame of the slider. With the consideration of thermal factors, the voice coil remains at a relatively low temperature during high-current driving tasks. The central part of the frame is cut through to reduce the eddy current effect, as shown in Fig. 2(b). The optical encoder is located in the centre of the VCM and is parallel to HR918UU guides. The encoder reader is embedded in the slider and assembled according to the technical requirement of the Renishaw. The customize VCM applied in this cutting device is a linear VCM, while the standard VCM operates in a rounded mode. The linear VCM has the advantage of a small form factor, which can drastically reduce the sliding mass, resulting in a higher system acceleration.

### 2.3. Mechanical design of the piezoelectric actuated flexure-hinge mechanism

The flexure-hinge mechanism is installed at the front of the slider and is connected, as shown in Fig. 1(a). The isolated view of the second-order mechanical system is demonstrated in Fig. 3. The specification of the piezoelectric actuator is shown in Table 1.

The capacitive sensor is installed at the top of the flexure-hinge structure by a float plate fixture connected to the VCM slider, as shown in Fig. 1(a). A thin metal plate is perpendicularly attached to the stroke direction with a short sensing distance (0.25 mm) to the sensing head of the capacitive sensor. The C8-3.2–2.0 probe works in conjunction with the second-order stroke to provide the nanoscale position feedback for the flexure-hinge compliant mechanism. The piezoelectric actuator is embedded in the centre of the flexure-hinge mechanism and preloaded by an M4 set screw, as shown in Fig. 3(a). A high-strength M2.5 screw holds the single-point diamond tool in place in a form notch.

## 3. Properties of the hybrid actuation cutting device

### 3.1. Properties of piezoelectric actuated flexure-hinge mechanism

The flexure-hinge utilizes a primary half-circular mechanism to simplify the manufacturing process and improve the mechanical tolerance performance of the final part. Physik Instrumente provides the stack multilayer piezoelectric actuator. The front end of

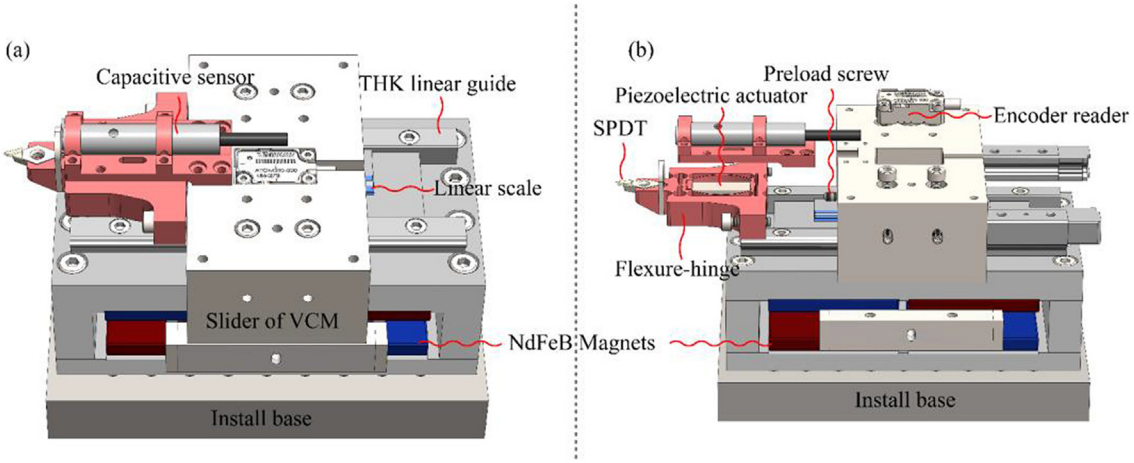


**Fig. 1.** Assembly view (a) and explored view (b) of the device.

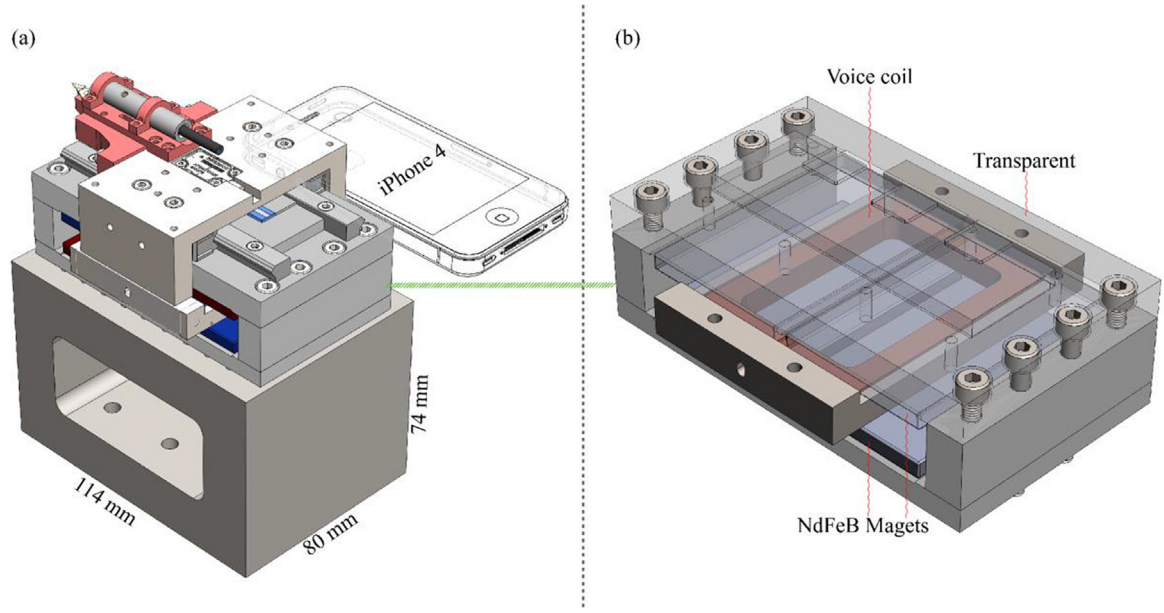


**Fig. 2.** A comparison of form factor between device and iPhone4 (a), and self-designed VCM (partial transparent, (b)).

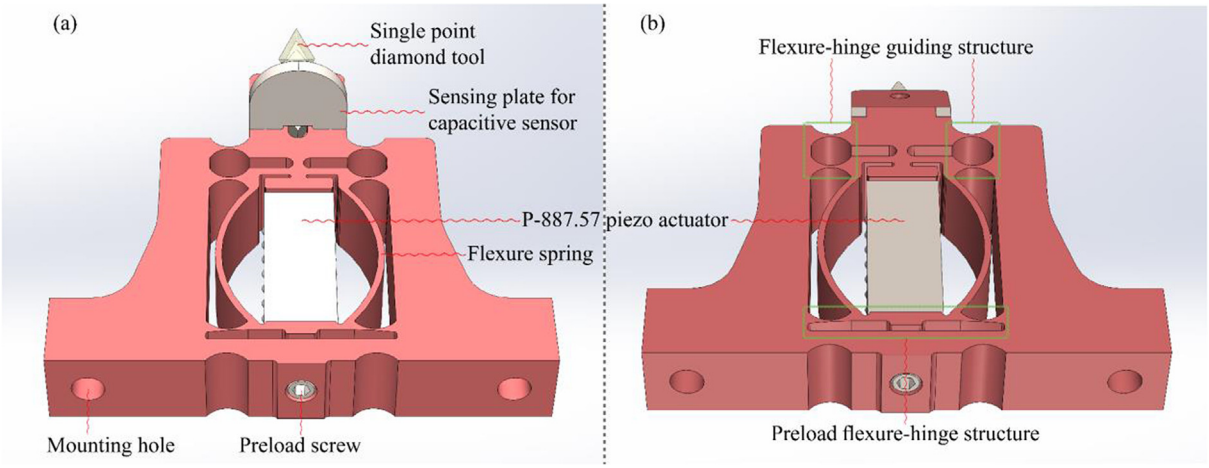


**Fig. 3.** Top (a) and bottom (b) view of the piezoelectric actuated flexure-hinge mechanism.

**Table 1**
Specifications of P-887.57 stack multilayer piezoelectric actuator.

| Dimensions L × W × H | Nominal travel range | Max. travel range | Blocking force | Stiffness | Electrical capacitance | Resonant frequency |
|---|---|---|---|---|---|---|
| 7 × 7 × 18 mm | 15 μm | 18 μm | 1750 N | 100 N/μm | 3.1 μF | 70 kHz |

the flexure hinge is connected to a flexure joint. The preload flexure is located at the end of the structure, as shown in Fig. 3(b), which is preloaded by a set screw through a thin flexure joint. The thin circle spring connected with the front end and bottom base enables to increase the dynamic performance of the instrument.

The whole static range of the flexure-hinge mechanism is validated by a series of commands in voltage (range from 0.5 V to 12 V, see Table 2.), which corresponds to 0 to 120 V amplitude output from the piezoelectric amplifier. Using the DC power supply to generate a voltage signal for the input port of the piezoelectric amplifier, the corresponding driving voltage is outputted to the piezoelectric actuator from the driver. The flexure-hinge guides the front end (single point diamond tool) to execute precise motions. In this experiment, the front sensing end is attached by a steel plane for a capacitive positioning sensor. The CPL290 and MM190 module perform the decoding task and return the absolute displacement deviation of the front tip of the whole flexure-hinge mechanism. The oscilloscope simultaneously acquires the voltage signal from the CPL290 auxiliary coaxial output.

The sensitivity of the capacitive sensor is 40.000 mV/μm when the sensitivity of CPL190 is set to low sensitivity. Then the calculated displacement of the compliant mechanism at the front flexure-hinge can be estimated as

$$Cr = \frac{Ud}{40.000} \tag{1}$$

**Table 2**
Static close-loop static travel performance test of flexure-hinge.

| Control In (V) | MM190 (μm) | $U_d$(mV) | Cr (μm) | DIV (μm) |
|---|---|---|---|---|
| 0.50 | 0.44 | 17.60 | 0.44 | 0.00 |
| 1.00 | 0.88 | 34.90 | 0.87 | −0.01 |
| 1.50 | 1.28 | 51.00 | 1.28 | −0.01 |
| 2.00 | 1.76 | 70.4 | 1.76 | 0.00 |
| 2.50 | 2.28 | 91.20 | 2.28 | 0.00 |
| 3.33 | 2.91 | 116.00 | 2.90 | −0.01 |
| 3.50 | 3.54 | 141.00 | 3.53 | −0.02 |
| 4.00 | 4.20 | 170.00 | 4.25 | 0.05 |
| 4.50 | 5.00 | 199.00 | 4.98 | −0.03 |
| 5.00 | 5.68 | 228.00 | 5.70 | 0.02 |
| 5.50 | 6.71 | 269.00 | 6.73 | 0.01 |
| 6.00 | 7.27 | 292.00 | 7.30 | 0.03 |
| 6.50 | 8.18 | 329.00 | 8.23 | 0.04 |
| 7.00 | 9.00 | 362.00 | 9.05 | 0.05 |
| 7.50 | 9.87 | 397.00 | 9.93 | 0.06 |
| 8.00 | 10.74 | 432.00 | 10.80 | 0.06 |
| 8.50 | 11.66 | 468.00 | 11.70 | 0.04 |
| 9.00 | 12.42 | 499.00 | 12.48 | 0.05 |
| 9.50 | 13.37 | 536.00 | 13.40 | 0.03 |
| 10.00 | 14.24 | 571.00 | 14.28 | 0.04 |
| 10.50 | 15.10 | 607.00 | 15.18 | 0.08 |
| 11.00 | 15.95 | 642.00 | 16.05 | 0.10 |
| 11.50 | 16.81 | 676.00 | 16.90 | 0.09 |
| 12.00 | 17.68 | 711.00 | 17.78 | 0.09 |

Note: Control In: drive command from the controller, MM190: capacitive position sensing end from LION Precision, $U_d$: Agilent digital oscilloscope sensing from CPL290 auxiliary output, Cr: Calculated result from DSO-X2024A voltage value and sensitivity, DIV: Deviation between calculation result and MM190 reader.

*Cr* and directed values shown in the MN190 module were grouped in Table 2. The DIV represents the deviation between Cr and MN190 value. The divergence of the two devices is small, ranging from −0.03 μm to 0.1 μm, as illustrated in Table 2.

### 3.2. Properties of voice coil motor actuated stroke mechanism

The first-order mechanism actuated by the VCM is designed to have a 30 mm stroke. The VCM is comprised of a square voice coil with 182 turns, a length of 62 mm and a width of 48 mm. The armature of the VCM is supported by 316L steel and firmly adhered with a high thermal conductivity adhesive resin. The wires are twisted and covered by metal meshes to improve the anti-electromagnetic interference performance. The coil's resistance is approximately 9.571 Ω. The inductance of the coil in the magnetic field is 2.99 mH. The properties of the voice coil are listed in Table 3.

This linear VCM employs four 60 × 40 × 4.3 mm square permanent magnets made from NdFeB, and the model is N50. In accordance with the Lorentz force law, the force is generated when applying the current is applied to the voice in the magnetic field. The relationship is represented by the simplified equation:

$$f = nBIl \tag{2}$$

where $f$ is Lorenz force, $n$ is the number of effective turns, $B$ is the average magnetic flux density, $I$ is represented the excitation current through the coil, and $l$ is the valid length to generate the Lorenz force. For this VCM, $n$ is 182 and $l$ is 62 mm and $B$ is about 0.125 T on average. Therefore, the continuous force of the VCM is approximately 14.21 N when applying 5A continuous current to the coil. A force sensor is employed to test static Lorenz force at every 2 mm pitch to determine the force value of the whole stroke, as shown in Fig. 4, and the result is shown in Fig. 5. The force constant of the VCM is about 2.84 N/A. As the peak current is double the continuous current, the VCM generates a peak force of 28.4 N.

## 4. Modelling and analysis of the hybrid actuation cutting device

### 4.1. Finite element validation of the flexure-hinge compliant mechanism

As the device is designed to generate high-accuracy and high-frequency micro/nanoscale strokes for micro/nanostructures in ultra-precision single-point diamond cutting, the stiffness and accuracy of flexure-hinge are the main consideration factors in achieving the intended working frequency. The flexure-hinge mechanism is made of aluminium alloy 6061-T6. The SolidWorks simulation module is used to conduct a finite element modal analysis based on the designed flexure-hinge model. The simulation result indicates that the first-order resonant frequency is 5006 Hz, as depicted in Fig. 6.

The capacitive sensor for sensing flexure-hinge displacement can be used to validate the simulation result. The schematic of the experimental setup is shown in Fig. 7. The excitation signal is generated by a microprocessor (STM F407) and amplified by an amplifier (E-617 LVPZT), finally detected by a high-accuracy capacitive position sensor. The embedded math function of the oscilloscope (DSO-X 2024A) calculates the fast Fourier transform (FFT). The inputs of the FFT are the voltage signal acquired from the CPL290 auxiliary output, which represents the deformation response of the flexure-hinge in response to the excitation input. The yellow signal on Channel 1 is the excitation signal, while the green signal is the position feedback of the capacitive sensor. Thus, when the persistence function is enabled, and the frequency exci-

**Table 3**
Properties of voice coil for the VCM.

| Frequency(*kHz*) | Voltage(*V*) | Induction(*mH*) | Resistance(Ω) | Turns | Dimension(*mm*) |
|---|---|---|---|---|---|
| 1.0 | 0.3 | 2.99 | 9.571 | 182 | 62 × 48 |

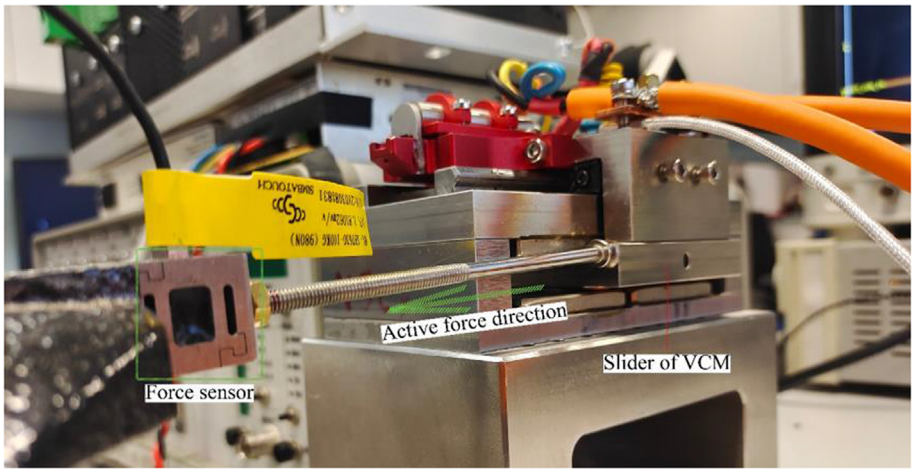


**Fig. 4.** Static Lorenz force test set up.

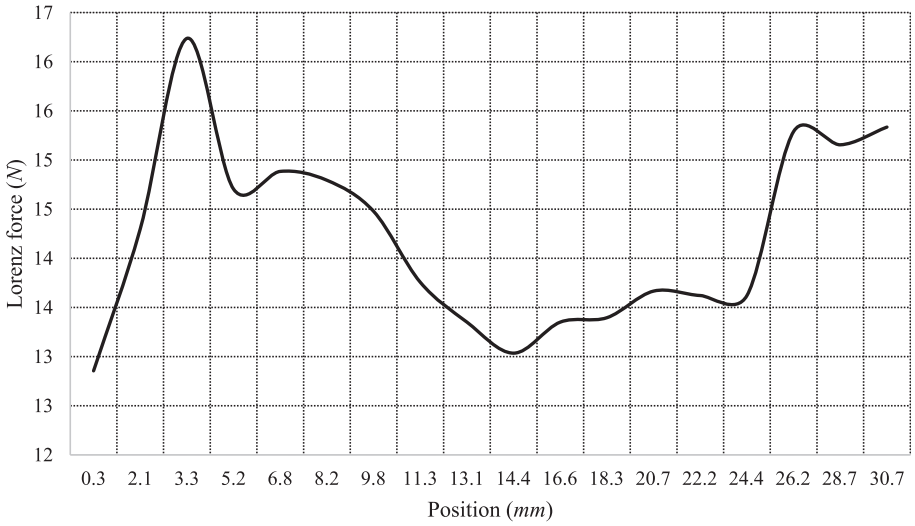


**Fig. 5.** Continuous Lorenz force curve of the customize VCM.

tation sweeps from 10 Hz to 20 kHz, the background color is green. FFT result is denoted by solid purple color, as shown in Fig. 7(b). Based on the modal simulation result, the first-order modal analysis result is 5006 Hz, as shown in Fig. 6, while the experimental result is about 5090 Hz, as shown in Fig. 7(b). The deviation is about 84 Hz, proving that the simulation results of the modal analysis performed by the embedded module of SolidWorks are accurate to within 1.6 %.

Fig. 7 shows the persistence plot of FFT, which is a collection of six frequency sweep excitations with a 1Vpp sine wave input and a 0.5 V offset. From the experimental and simulated modal analyses, the flexure-hinge mechanism has a bandwidth of approximately 5000 Hz. The designed working bandwidth is set to 3300 Hz to prevent unstable vibration in the cutting process. The simulated results for the second to fifth-order resonant frequencies are shown in Fig. 8. They are 8216 Hz, 11472 Hz, 12244 Hz, and 12455 Hz, respectively.

### *4.2. Magnetic field simulation of linear voice coil motor*

In order to optimize the design of the VCM, magnetic field simulation is performed with the SolidWorks add-in module for magnetic simulations. The simulation setup is shown in Fig. 9. The dark blue arrow indicates the magnetic direction of the NdFeB permanent magnet, whereas the green arrow indicates the voice coil's current direction. The stator of the VCM is made of 304 stainless steel, and the NdFeB uses the model N55, which has residual induction of 1.49 T in nominal conditions for simulation. The magnetic field simulation results are shown in Fig. 10, and the flux density is about 0.187 T on average, generating a Lorentz force of 18 N under the current condition of 7A with the 110-turn coil, according to Eq. (2).

The simulation result of the Lorentz force is larger than the actual force output from the device. Table 4 illustrates the distinction between the simulation and the actual setup. Effective magnetic flux density is the key factor that influences the output Lorentz force value, while the residual induction of the NdFeB determines the effective magnetic flux density. Although the simulation (7A) and actual setup (5A) have different excitation conditions, both output Lorentz forces are accurate, providing guidance for optimizing the design to improve high-frequency dynamic performance.

## 5. Performance test of the hybrid actuation cutting device

The final assembly of the device with the single diamond point tool is depicted in Fig. 11; the red front portion represents the first-order flexure-hinge mechanism. The electrical connector used for

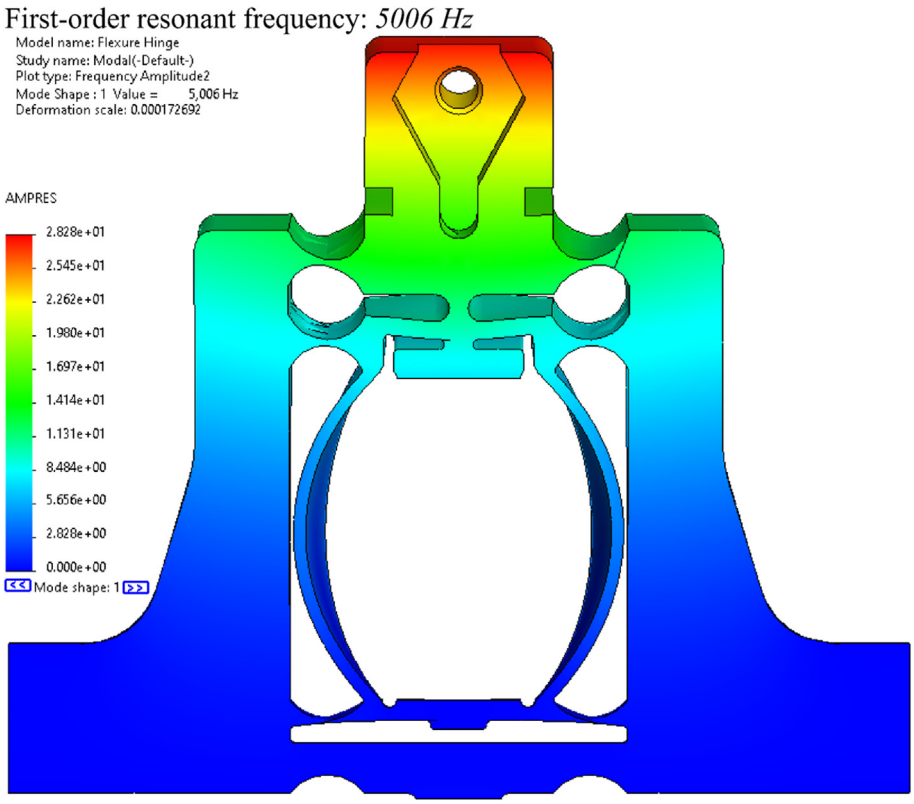


**Fig. 6.** First-order modal analysis results of flexure-hinge mechanism.

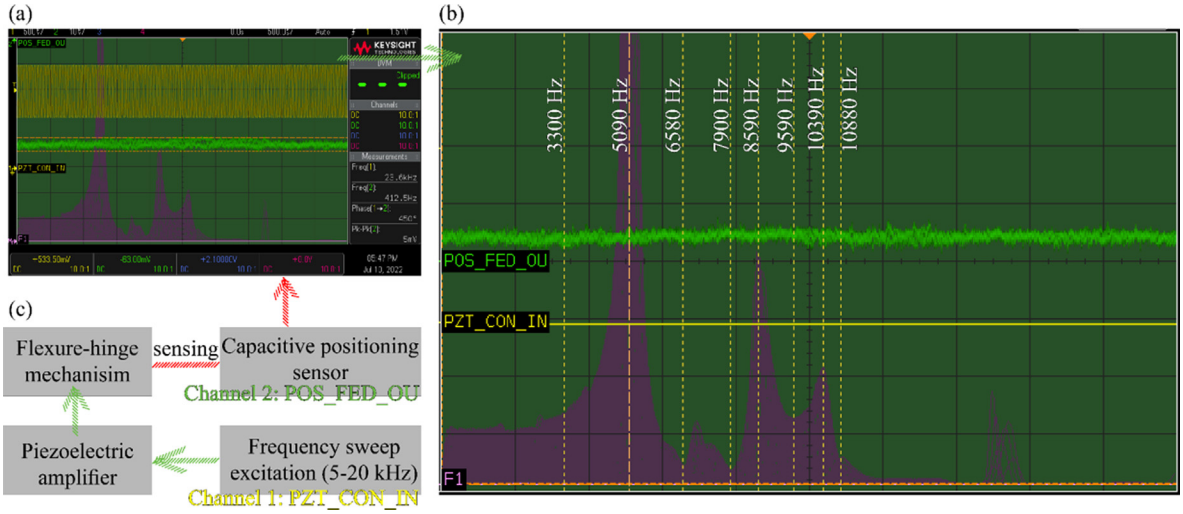


**Fig. 7.** (a). FFT persistence result of the flexure-hinge response from 1 V sine excitation (10 Hz-20KHz) by an oscilloscope (5.09KHz for experimental first-order modal), (b). enlarge view of the results, and (c). schematic of the validated experimental setup.

the piezoelectric actuator and VCM consists of a 2 mm circular reliable connector, shielded cable for the VCM, and coaxial cable for the piezoelectric actuator.

Fig. 12 shows the experimental current excitation in step mode, where the blue curve represents the actual current value passing through the coil, and the green line represents the desired current command generated by the amplifier. Based on the plotted results, the performance of the current close loop is validated. Utilizing the Renishaw 20 μm pitch linear encoder system, the VCM-driven slider can perform precise strokes for servo control. Fig. 13 proves the accuracy of the VCM actuated slide, where the position error is within 2 μm. The driver instructs the slider to produce a 50 Hz sine wave stroke with an amplitude of 50 μm. The figure shown in Fig. 13(a) is the actual motion curve (blue curve) and position error (green line). Fig. 13(b) is the enlarged view of the position error (green line). Fig. 14 shows the stroke result of the VCM slide with the parameters at ± 0.5 mm (10 Hz) in sine mode.

As mentioned above, the designed working frequency of the flexure-hinge is set to 3300 Hz. In order to validate the performance of the front-end mechanism (the experimental setup is shown in Fig. 15), a series of experimental parameters are developed. This mechanism is mainly for microstructure generation in

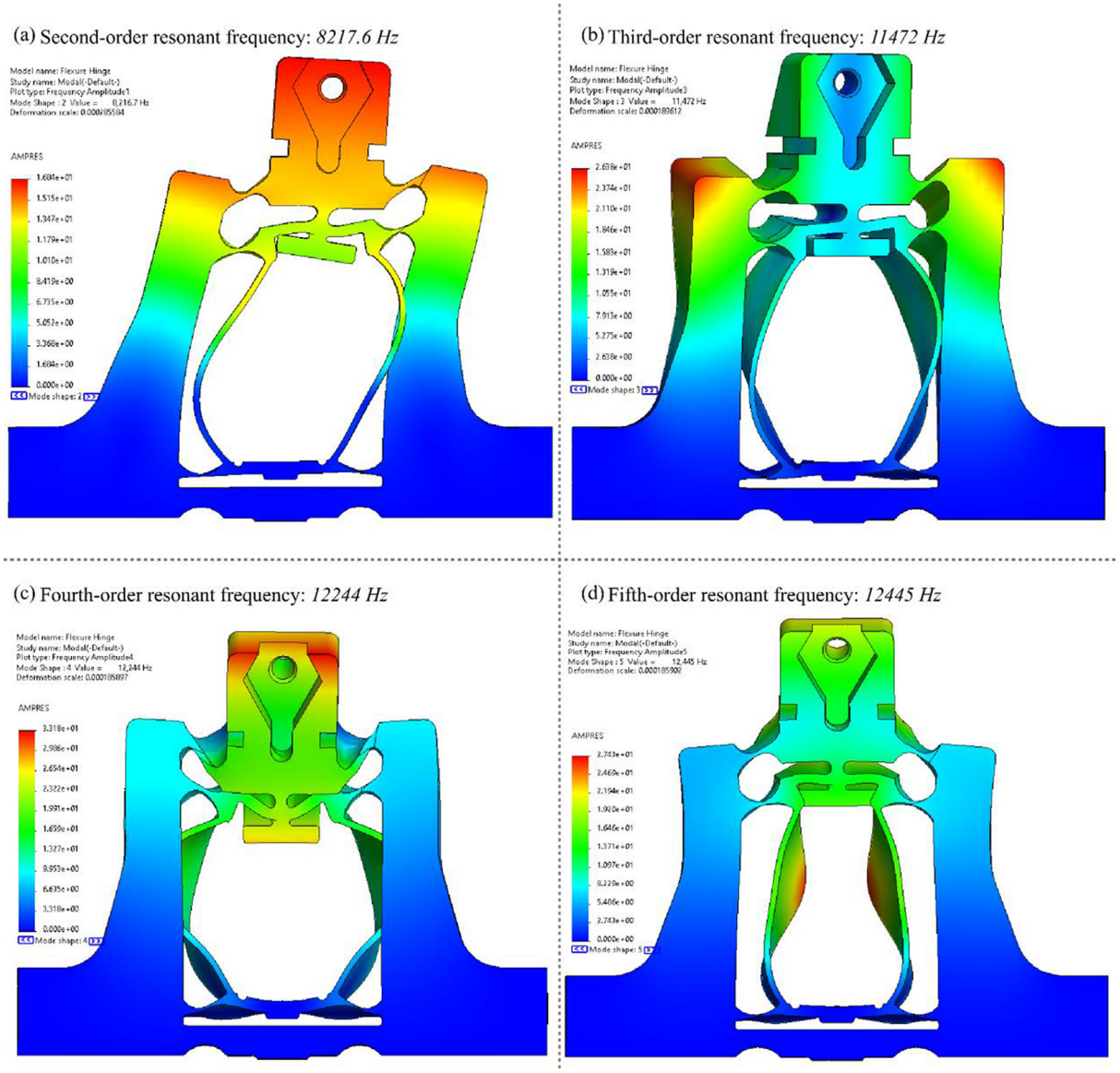


**Fig. 8.** The rest four modal analysis results (Second- to fifth-order).

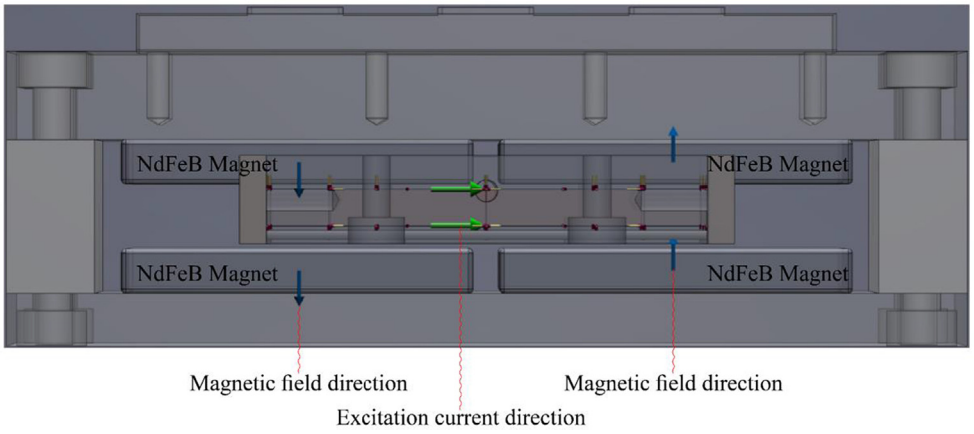


**Fig. 9.** Magnetic simulation set up of the VCM.

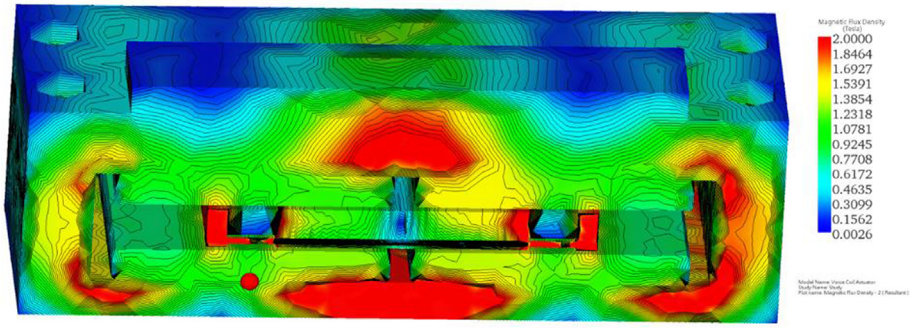


**Fig. 10.** Section view of VCM magnetic field simulation result (4 × N55 NdFeB).

**Table 4**
Difference between simulation and actual setup in different parameters.

| | NdFeB magnets model | Turns of the coil | Magnetic flux density | Lorentz force |
|---|---|---|---|---|
| Simulation | N55 | 110 | 0.187 T | 17.90 N |
| Actual setup | N50 | 182 | 0.125 T | 14.21 N |

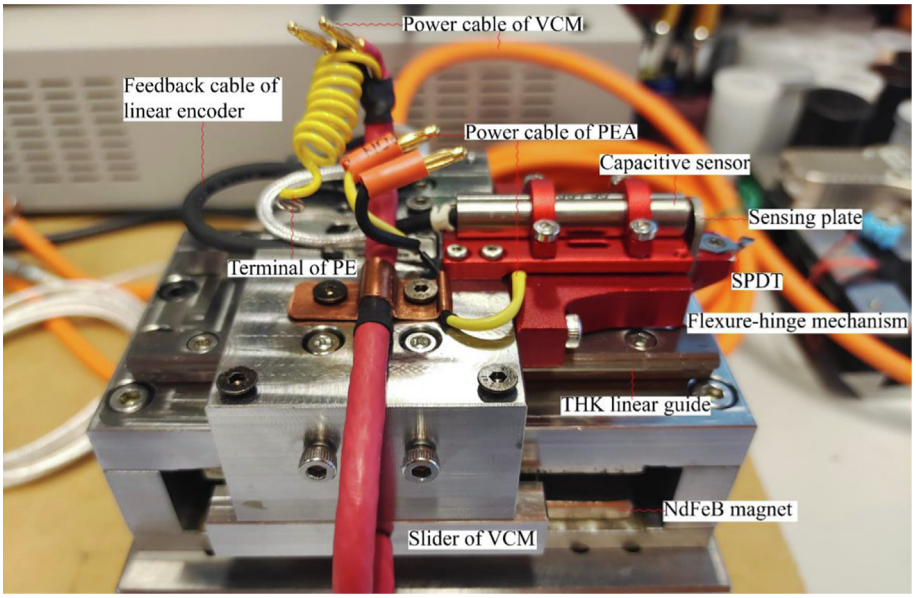


**Fig. 11.** Actual assembly view of the device (PE: Protect earth; SPDT: single point diamond tool; PEA: Piezoelectric actuator; VCM: voice coil motor).

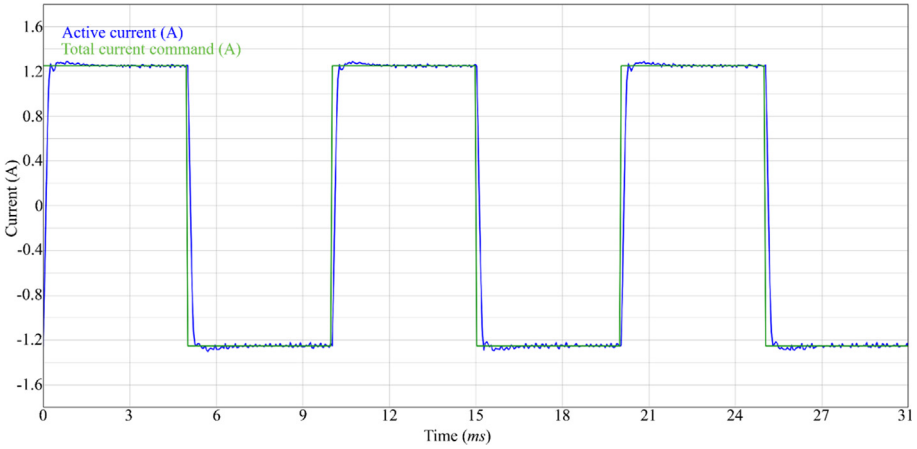


**Fig. 12.** Current step response and validation of current command.

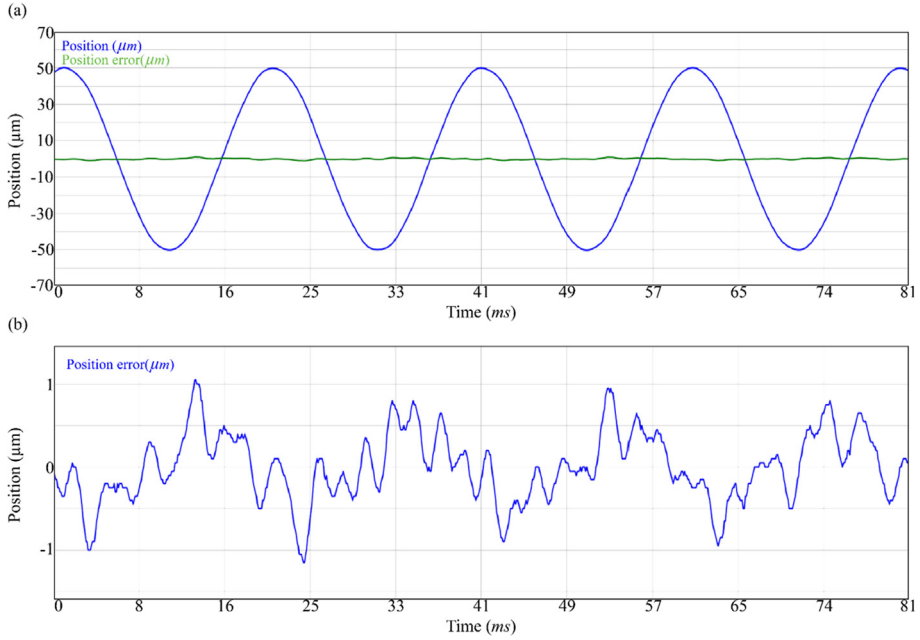


**Fig. 13.** Position error (a) with sine motion (50 Hz @ Amplitude 0.05 mm) and (b) enlarge view of position error.

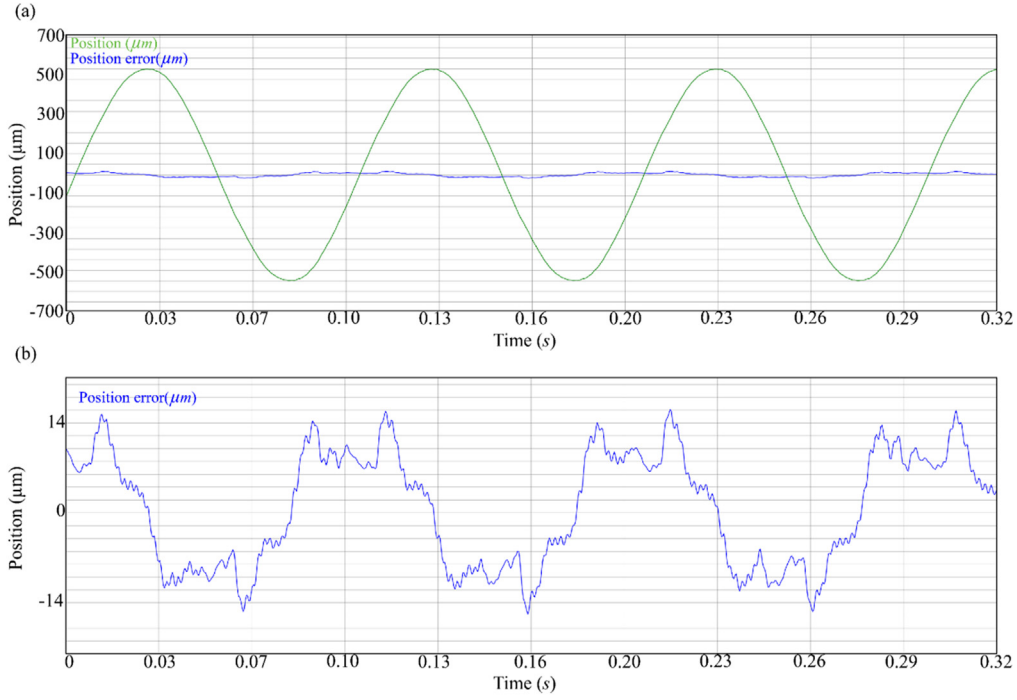


**Fig. 14.** Position error (a) with sine motion (10 Hz @ Amplitude 0.5 mm) and (b) enlarge view of position error.

micro stroke. Two groups of different cutting parameters, as shown in Table 5, are designed. The variable is the vibration frequency and the diameter of a dimple (DoD), as shown in Table 5. The first group experiment adopts different frequencies of the piezoelectric actuator, beginning with the 400 Hz and increasing with the pitch of 400 Hz until the designed maximum working bandwidth. The spindle speed and cutting time are calculated to generate a micro dimple with a circular distribution, given that the diameter of the workpiece is 8 mm, and the material is copper.

For the first group experiments, the amplitude of the sine wave is set to 330 mV, representing a 2.9 μm stroke of the front end of the diamond tool. To achieve the desired number of spherical-like microstructures, the spindle speed and cutting time vary based on the distance to the rotating centre. The actual cutting parameters are displayed in Table 5.

## 6. Experimental results and discussion of microstructure generation

In order to validate the stiffness performance of the cutting device, two samples are machined by a standard ultra-precision turning process with the second-order flexure-hinge mechanism

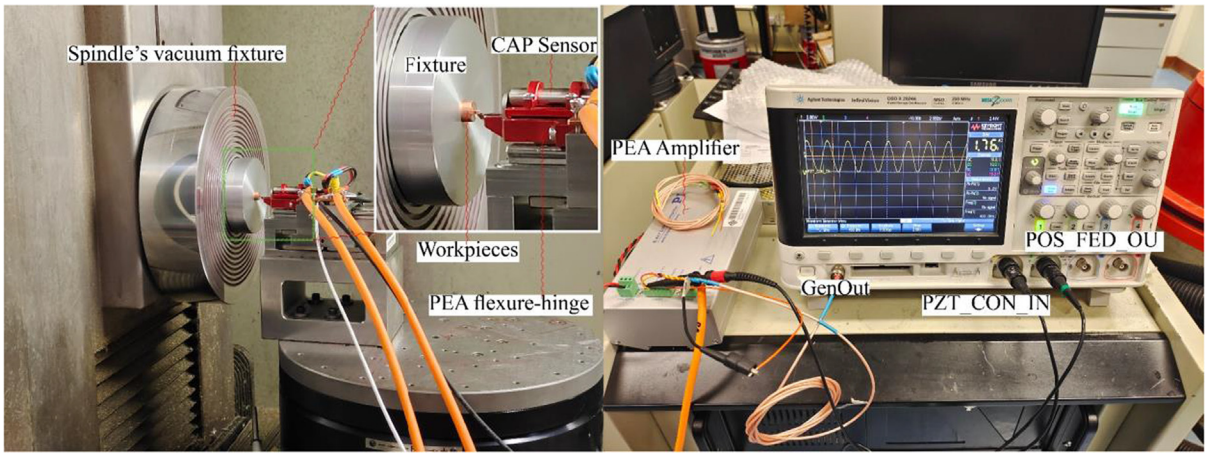


**Fig. 15.** Experimental setup for the validation of the flexure-hinge mechanism.

**Table 5**
Designed experiment for flexure-hinge mechanism validation with different cutting parameters.

| Fre (*Hz*) | DoC (*mm*) | DoD (*mm*) | SS (*RPM*) | DtC (*mm*) |
|---|---|---|---|---|
| 400 | 0.0029 | 0.074393 | 87.59 | 3.2442 |
| 800 | | | 181.82 | 3.1258 |
| 1200 | | | 295.08 | 2.8890 |
| 1600 | | | 410.25 | 2.7706 |
| 2000 | | | 535.71 | 2.6522 |
| 3300 | | | 920.93 | 2.5456 |
| 2500 | 0.0004 | 0.029052 | 214.90 | 3.2274 |
| | 0.0009 | 0.041067 | 313.81 | 3.1242 |
| | 0.0013 | 0.049508 | 400.00 | 2.9548 |
| | 0.0018 | 0.058024 | 487.02 | 2.8443 |
| | 0.0023 | 0.066006 | 574.70 | 2.7419 |
| | 0.0029 | 0.074393 | 672.65 | 2.6403 |
| | 0.0035 | 0.082138 | 769.22 | 2.5492 |

Note: Fre: frequency; DoC: depth of cut; DoD: diameter of dimple; SS: spindle speed; DtC: distance to centre.

and VCM-driven slider. Fig. 16 shows the machined surface topographies of the machined surfaces. Both surface roughness is about 3 nm. Fig. 16(a) is the surface finishing result of the second-order flexure-hinge mechanism, while Fig. 16(b) is the high-quality surface generated by VCM driven slider separately. This means the VCM slider, and the flexure-hinge mechanism are actuated by a preload driving voltage to hold a standstill in an actual position. The experiment proves that both mechanisms achieve the ultra-precision machining requirement.

Two samples were machined using two groups of cutting parameters to validate the frequency and amplitude domain based on the designed experiments for the flexure-hinge mechanism. The 3D profile result of one cutting condition is shown in Fig. 17, and the rest profile results are demonstrated in Table 6 and Table 7. The actual depth of cut is 2.422 μm compared to the command value of 2.9 μm, and the active vibration frequency is 2510.56 Hz which can be calculated from the pitch value as shown in Fig. 17 (b). The command and active frequency deviation is only 10.56 Hz (0.42 %), as illustrated in Table 5. The designed DoD of this example is 74.393 μm, while the actual DoD is 74.289 μm. The error ratio in the DoD value is only 0.12 %. The detailed experimental results for frequencies from 400 Hz to 3300 Hz are shown in Table 6. The active frequency can be calculated from the actual pitch, distance to centre and spindle speed. The relationship between those parameters is shown below:

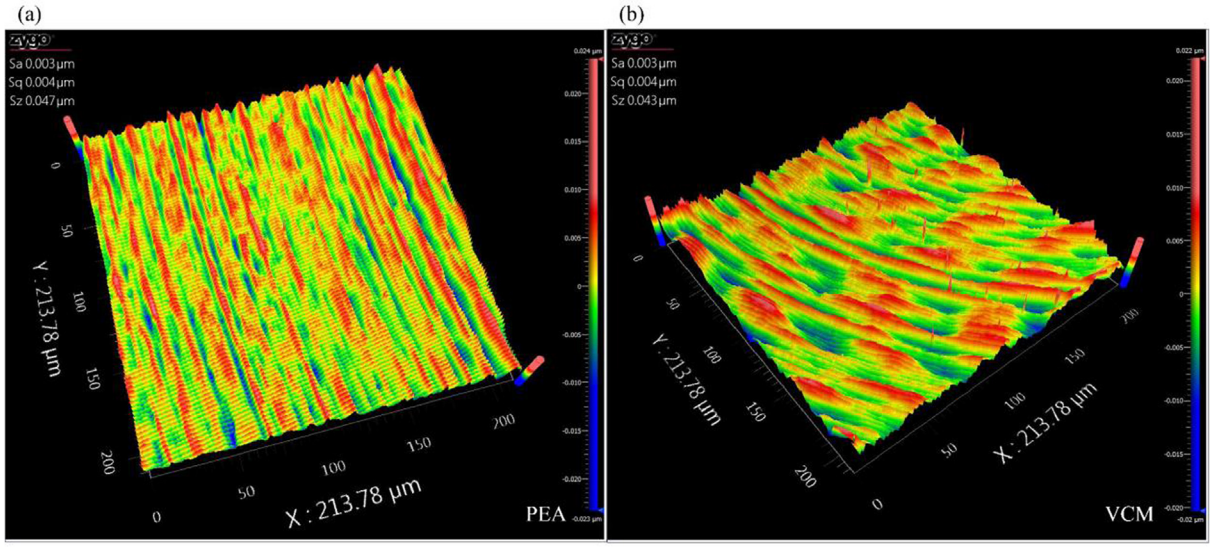


**Fig. 16.** Stiffness validation of (a) piezoelectric actuated (PEA) and (b) VCM-driven slider by manufacturing an excellent surface.

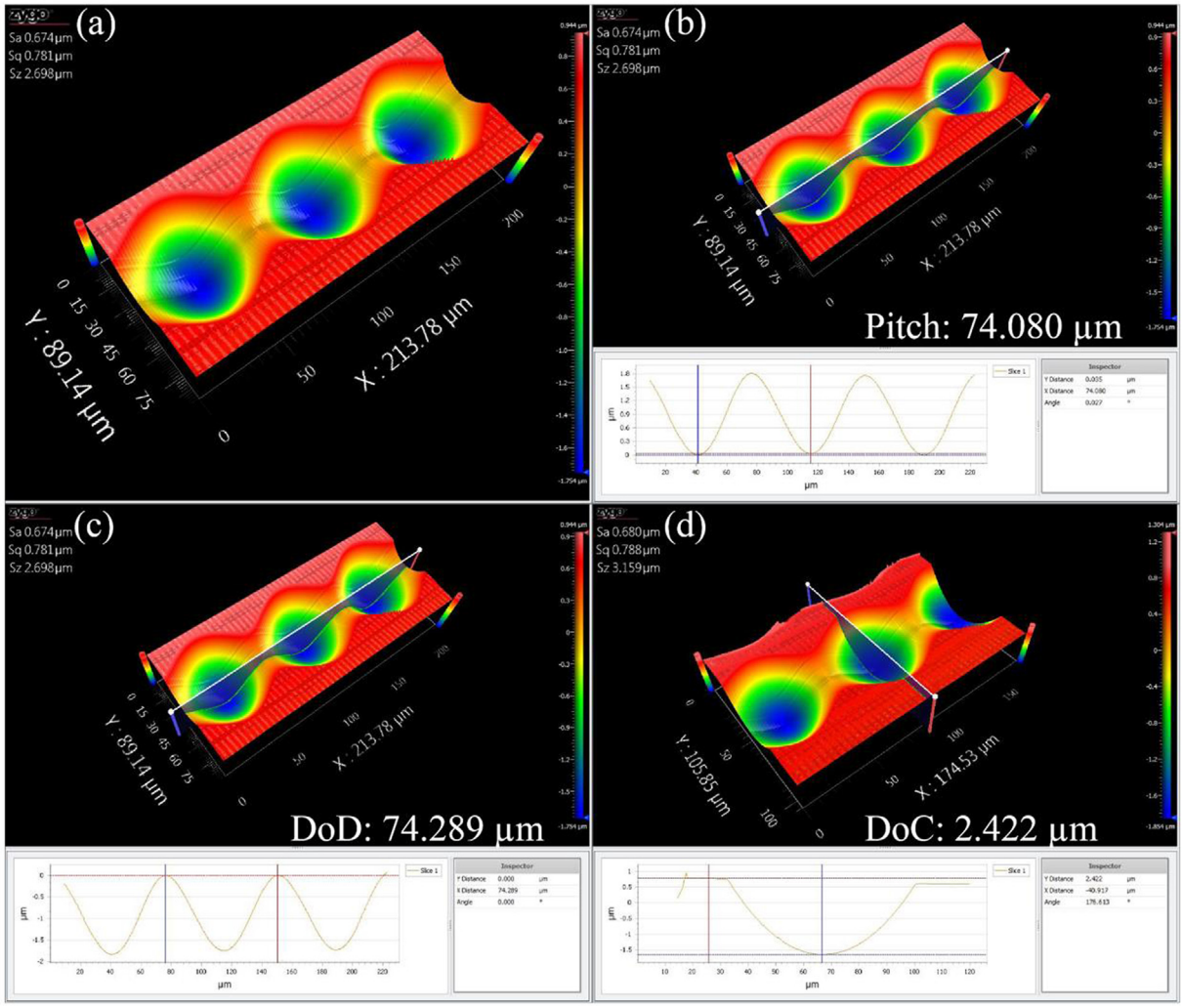


**Fig. 17.** Profile example of cutting parameters with frequency at 2500 Hz, DoC at 0.0029 mm and SS at 672.65 RPM; (a) 3D profile of the microstructure; (b) pitch value of two dimple structures; (c) diameter of single dimple microstructure and (d) depth of cut of the microstructure.

**Table 6**
Active vibrated frequency calculated from profiled pitch value (DoC at 0.0029 mm).

| Designed frequency (Hz) | 400 | 800 | 1200 | 1600 | 2000 | 3300 |
|---|---|---|---|---|---|---|
| Active frequency (Hz)* | −2.27 | +17.15 | −27.16 | −10.8 | +101.36 | −56.64 |
| Actual pitch (µm) | 74.817 | 72.833 | 76.116 | 74.898 | 70.805 | 75.692 |
| Distance to centre (mm) | 3.2442 | 3.1258 | 2.8890 | 2.7706 | 2.6522 | 2.5456 |
| Spindle speed (RPM) | 87.59 | 181.82 | 295.08 | 410.25 | 535.71 | 920.93 |

*Note: The value of active frequency is the deviation compared to the designed frequency.

**Table 7**
Active vibrated frequency of different DoC calculated from profiled pitch value (Frequency at 2500 Hz).

| Designed DoD (µm) | 29.052 | 41.067 | 49.508 | 58.024 | 66.006 | 74.393 | 82.138 |
|---|---|---|---|---|---|---|---|
| Actual DoD (µm)* | −3.153 | −1.829 | −0.005 | −0.223 | 1.188 | −0.104 | 0.085 |
| DoD percentage error | −10.85 % | −4.45 % | −0.01 % | −0.38 % | 1.80 % | −0.14 % | 0.10 % |
| Designed DoC (µm) | 0.400 | 0.900 | 1.300 | 1.800 | 2.300 | 2.900 | 3.500 |
| Actual DoC (µm)* | −0.188 | −0.131 | −0.321 | −0.480 | 0.673 | −0.478 | 1.642 |
| DoC percentage error | −47.0 % | −14.6 % | −24.7 % | −26.7 % | 29.3 % | −16.5 % | 46.9 % |
| Actual pitch (µm) | 29.659 | 41.325 | 48.876 | 58.427 | 66.150 | 74.080 | 82.014 |
| Distance to centre (mm) | 3.2274 | 3.1242 | 2.9548 | 2.8443 | 2.7419 | 2.6403 | 2.6403 |
| Spindle speed (RPM) | 214.90 | 313.81 | 400.00 | 487.02 | 574.70 | 672.65 | 769.22 |
| Designed Frequency (Hz) | 2500 | | | | | | |
| Actual Frequency (Hz)* | −51.155 | −15.601 | 32.334 | −17.226 | −5.454 | 10.557 | 3.774 |

*Note: The value of active value is the deviation compared to the designed value.

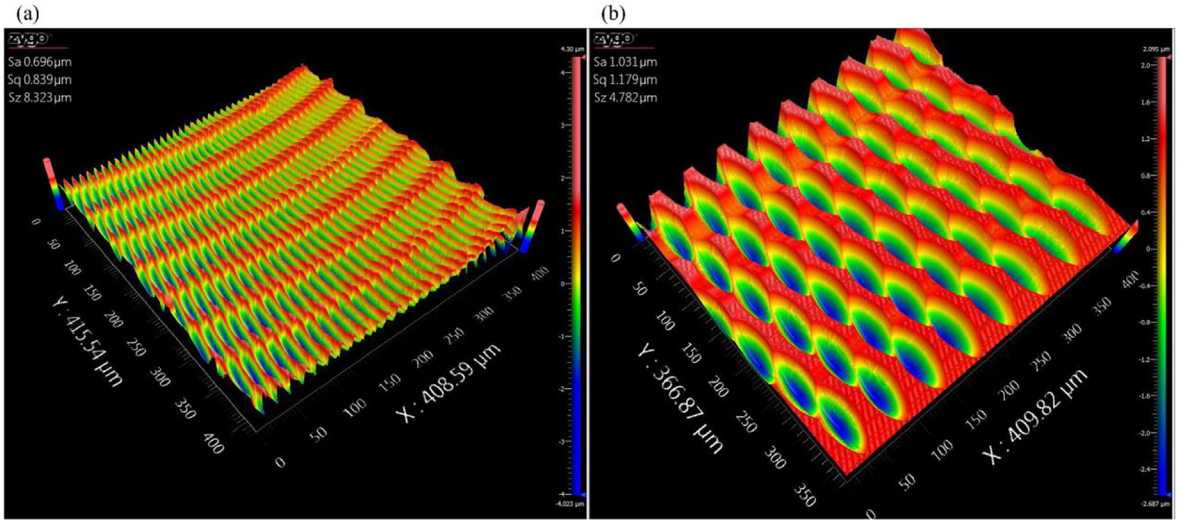


**Fig. 18.** Microstructure generated by the second-order flexure-hinge mechanism, (a) surface morphology near rotation centre and (b) outer area.

**Table 8**
Active frequency validated experiment for VCM-driven stroke system.

| Designed frequency (Hz) | 20 | 50 | 100 |
|---|---|---|---|
| Active frequency (Hz)* | −0.42 | −0.78 | / |
| Actual pitch (µm) | 138.877 | 168.528 | 86.306 |
| Feed rate in X direction (mm/min) | / | / | 3 |
| Distance to centre (mm) | 3.2442 | 3.6000 | / |
| Spindle speed (RPM) | 8 | 22 | 27 |

*Note: The value of active value is the deviation compared to the designed value.

$$Activefrequuency = \frac{SpindleSpeed \times \frac{2\pi}{60} \times Distancetocenter}{Actualpitch} \quad (3)$$

The deviation in the first series of experiment in the frequency field ranges from −56.64 to 101.36 Hz. The error ratio ranges from −2.26 % to 5.07 % and 0.33 % on average. Considering the different depths of cut, the error ratio in the frequency domain is about −0.24 % on average, as listed in Table 7). The position error in the direction of depth ranges from 131 nm to 1.642 µm, while the designed depth of cut gradually increases from 400 nm to 3.5 µm at the working bandwidth of 2500 Hz in open loop mode. Fig. 18 shows the microstructure generated by the flexure-hinge mechanism using conventional turning technology at a feed rate of 8 mm/min. The profile reveals that the microstructures are distributed uniformly, as shown in Fig. 18.

Three different series of cutting parameters are prepared for the validation of the VCM-driven mechanism, as listed in Table 8. The relationship between those parameters is described by equation (3). The active frequency calculated through the experiment is 19.58 Hz and 49.22 Hz, and the 3D profile result is shown in Fig. 19. The third experiment with a stroke frequency of 100 Hz starts cutting at the position 3 mm away from the centre of the workpiece at a feed rate of 3 mm/min. The morphological characterization of the generated microstructure is demonstrated in Fig. 20, with the actual depth of cut being 6.441 µm. Given that the designed amplitude of sine wave stroke is 6 µm, the position error in stroke direction is 0.441 µm.

## 7. Conclusions

This research was undertaken to design a high-performance hybrid actuation cutting device for ultra-precision machining and evaluate the performance in the microstructure generation. A customized linear VCM is designed and optimized through the mag-

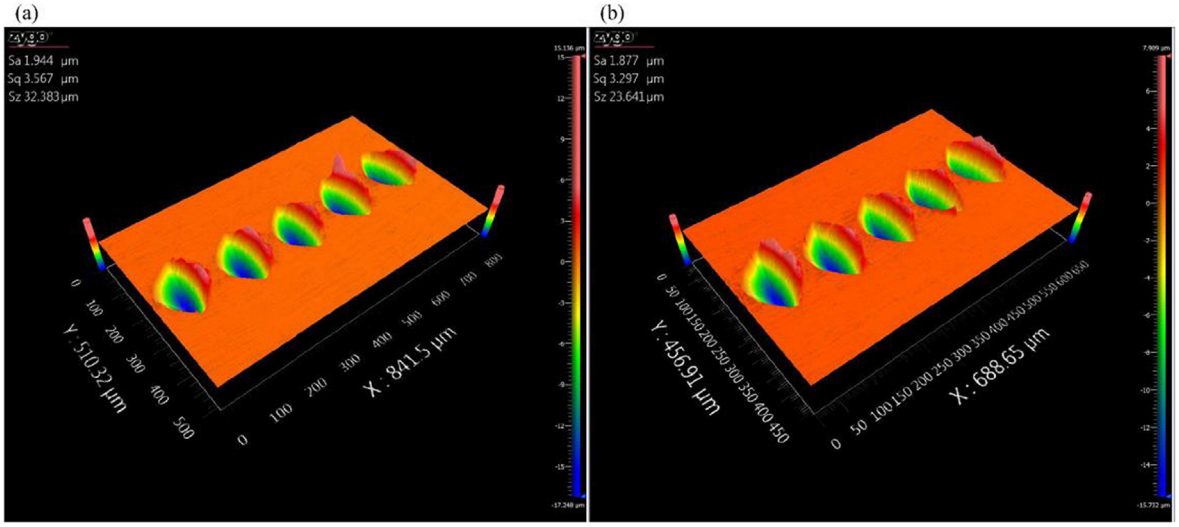


**Fig. 19.** Frequency validation for VCM-driven slider (a) sine frequency at 20 Hz and (b) sine frequency at 50 Hz.

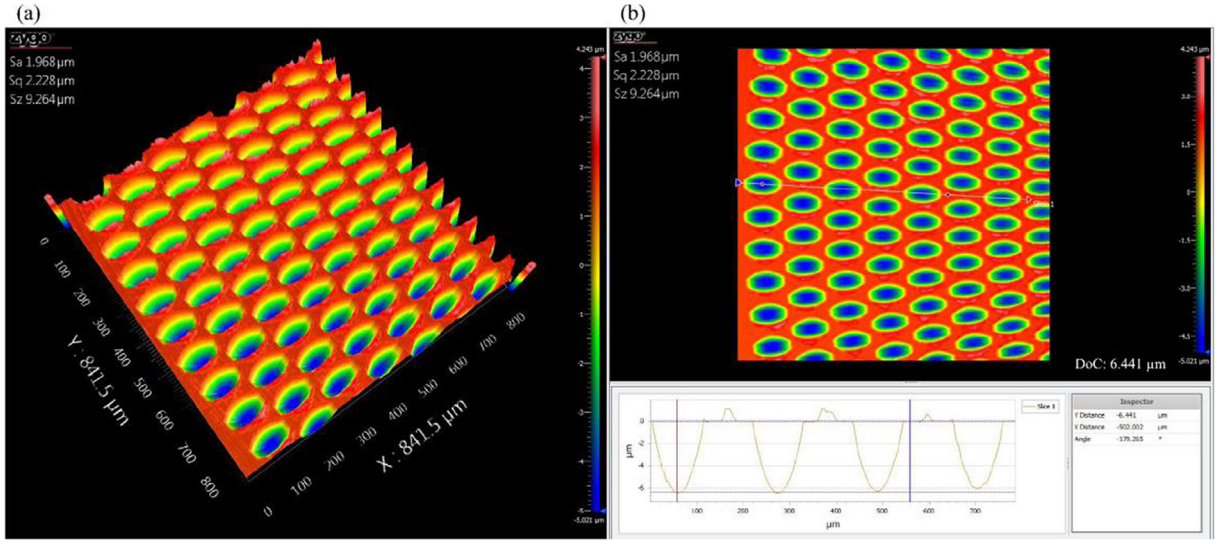


**Fig. 20.** Microstructure generated by VCM-driven first-order mechanism (a) 3D profile and (b) Depth of cut of the microstructure.

netic simulation technique. Meanwhile, the flexure-hinge compliant system is developed and validated by finite element analysis. After validating the working frequency of the flexure-hinge compliant subsystem with a modal analysis experiment, the constant force curve of the VCM is measured. The current step response and sine stroke tracking of the VCM actuation system are verified. Finally, a series of designed experiments are conducted to determine the performance of the hybrid actuation cutting device. The hybrid actuation cutting system presented here is one of the first investigations to explore high frequency cutting performance by generating microstructure surfaces in ultra-precision machining with high accuracy and flexibility. The significant contributions of this study are concluded as follows:

1. A compact mechanical design of a high-performance hybrid cutting system with a piezoelectric actuator and VCM is presented. This study has found that, generally, hybrid actuation is idealized for the generation of microstructures.

2. The sine stroke tracking experiment has validated the performance of the VCM, and the position error (amplitude of ± 0.05 mm and frequency at 50 Hz) is approximately ± 0.001 mm. The flat surface roughness generated by the VCM-driven slider is 3 nm.

3. The experiment demonstrates the superior frequency accuracy of the flexure-hinge compliant mechanism with an error ratio of 0.42 % at 2500 Hz. The working frequency can reach up to 3300 Hz, the first natural frequency is 5090 Hz, and the stroke of the flexure-hinge compliant mechanism without an amplifier is 17.78 µm.

4. A series of microstructure generation experiments are conducted on the designed device to validate the cutting performance. The experiment results demonstrate a good agreement with the designed cutting parameters.

## Data availability

Data will be made available on request.

## Declaration of Competing Interest

The authors declare that they have no known competing financial interests or personal relationships that could have appeared to influence the work reported in this paper.

## Acknowledgements

The work described in this paper was partially supported by the Research Committee of The Hong Kong Polytechnic University (Account Code: RUWN and 4.45.XX.R006), State Key Laboratory of Ultraprecision Machining Technology, the Research Grants Council of the Hong Kong Special Administrative Region, China (15221322), the National Natural Science Foundation of China (U19A20104) and Sichuan Science and Technology Program (2020YFH006).

## References

[1] Z. Tong, W. Zhong, S. To, W. Zeng, Fast-tool-servo micro-grooving freeform surfaces with embedded metrology, CIRP Ann. 69 (2020) 505–508.
[2] P. Huang, X. Wu, S. To, L. Zhu, Z. Zhu, Deterioration of form accuracy induced by servo dynamics errors and real-time compensation for slow tool servo diamond turning of complex-shaped optics, Int. J. Mach. Tools Manuf. 154 (2020).
[3] D.L. Trumper, X. Lu, Fast tool servos: advances in precision, acceleration, and bandwidth, Towards Synthesis of Micro-/Nano-systems, Springer, 2007, pp. 11-19.
[4] Z. Lyu, Z. Wu, Q. Xu, Design and development of a novel piezoelectrically actuated asymmetrical flexible microgripper, Mech. Mach. Theory 171 (2022).
[5] M. Ling, L. Yuan, Z. Luo, T. Huang, X. Zhang, Enhancing Dynamic Bandwidth of Amplified Piezoelectric Actuators by a Hybrid Lever and Bridge-Type Compliant Mechanism, Actuators 11 (2022).
[6] F. Chen, Q. Zhang, Y. Gao, W. Dong, Design and Analysis of a Compact Piezo-Actuated Microgripper With a Large Amplification Ratio, Journal of Mechanical Design, Trans. ASME 144 (2022).
[7] F. Chen, Q. Zhang, W. Dong, L. Sun, Design and test of a compact large-stroke dual-drive linear-motion system, Mech. Syst. Signal. Process 180 (2022).
[8] C.N. Wang, F.C. Yang, V.T.T. Nguyen, Q.M. Nguyen, N.T. Huynh, T.T. Huynh, Optimal design for compliant mechanism flexure hinges: Bridge-type, Micromachines 12 (2021).
[9] F. Wang, Z. Huo, C. Liang, B. Shi, Y. Tian, X. Zhao, D. Zhang, A Novel Actuator-Internal Micro/Nano Positioning Stage with an Arch-Shape Bridge-Type Amplifier, IEEE Trans. Ind. Electron. 66 (2019) 9161–9172.
[10] Z. Gong, D. Huo, Z. Niu, W. Chen, K. Cheng, A novel long-stroke fast tool servo system with counterbalance and its application to the ultra-precision machining of microstructured surfaces, Mech. Syst. Signal. Process 173 (2022).
[11] Z. Gong, D. Huo, Z. Niu, W. Chen, K. Cheng, Dynamic performance of a long-stroke fast tool servo system, Nami Jishu yu Jingmi Gongcheng 5 (2022).
[12] Z. Zhu, H. Du, R. Zhou, P. Huang, W.L. Zhu, P. Guo, Design and trajectory tracking of a nanometric ultra-fast tool servo, IEEE Trans. Ind. Electron. 67 (2020) 432–441.
[13] F. Tian, Z. Yin, S. Li, A novel long range fast tool servo for diamond turning, Int. J. Adv. Manuf. Technol. 86 (2016) 1227–1234.
[14] F. Tian, Z. Yin, S. Li, Performance testing of a fast tool servo system driven by a voice coil motor, Guofang Keji Daxue Xuebao 37 (2015) 12–16.

[15] Y. Tao, Y.L. Chen, P. Hu, B.F. Ju, H. Du, Development of a voice coil motor based fast tool servo with a function of self-sensing of cutting forces, Precis. Eng. 65 (2020) 130–137.
[16] R. Zhou, Z.H. Zhu, L. Kong, X. Yang, L. Zhu, Z. Zhu, Development of a High-Performance Force Sensing Fast Tool Servo, IEEE Trans. Ind. Inf. 18 (2022) 35–45.
[17] C.F. Hsu, K.Y. Wong, Online constructive fuzzy sliding-mode control for voice coil motors, Appl. Soft Comput. J. 47 (2016) 415–423.
[18] Z. Yang, Y. Bai, S. Wang, X. Chen, Q. Liu, K. Li, H. Wang, X. Chen, The development of an displacement sensor embedded voice coil motor based fast-tool-servo for the machining of micro-structure, 5th International Conference on Asian Society for Precision Engineering and Nanotechnology, ASPEN 2013, Trans Tech Publications Ltd, Taipei, 2015, pp. 258-261.
[19] D. Wu, K. Chen, X. Wang, Tracking control and active disturbance rejection with application to noncircular machining, Int. J. Mach. Tools Manuf. 47 (2007) 2207–2217.
[20] F.J. Tian, Z.Q. Yin, S.Y. Li, Design and control of a novel fast tool servo used in diamond turning of freeform optics, in: C. Xin, L. Wingbun, L. Qiang, C. ChiFai, T. Suet, W. Sujuan (Eds.) 4th Asia Pacific Conference on Optics Manufacture, APCOM 2014, Trans Tech Publications Ltd, 2016, pp. 73-78.
[21] H. Li, H. Tang, J. Li, X. Chen, Design, fabrication, and testing of a 3-DOF piezo fast tool servo for microstructure machining, Precis. Eng. 72 (2021) 756–768.
[22] Z. Zhu, Z. Tong, S. To, X. Jiang, Tuned diamond turning of micro-structured surfaces on brittle materials for the improvement of machining efficiency, CIRP Ann 68 (2019) 559–562.
[23] R. Zhou, Y. Li, Y. Ji, L. Chen, L. Kong, Z. Zhu, Design and Control of a Hybrid Actuation Based Long Range Fast Tool Servo, Jixie Gongcheng Xuebao 55 (2019) 199–207.
[24] K.M. Chang, J.L. Cheng, Y.T. Liu, Machining control of non-axisymmetric aspheric surface based on piezoelectric fast tool servo system, Precis Eng. 76 (2022) 160–172.
[25] Z. Li, C. Guan, Y. Dai, S. Xue, L. Yin, Comprehensive design method of a high-frequency-response fast tool servo system based on a full-frequency error control algorithm, Micromachines 12 (2021).
[26] Z. Gong, D. Huo, Z. Niu, W. Chen, I. Shyha, Investigation of control algorithm for long-stroke fast tool servo system, Precis. Eng. 75 (2022) 12–23.
[27] Z. Gong, D. Huo, Z. Niu, W. Chen, K. Cheng, Robustness evaluation of control algorithms for a long-stroke fast tool servo, J. Manuf. Processes 80 (2022) 458–468.